



## LJMU Research Online

Ahuir Torres, JI, Kotadia, HR and Opoz, TT

**Effect of the electrical discharge machining on Ti6Al4V corrosion behaviour in simulated body fluid**

<http://researchonline.ljmu.ac.uk/id/eprint/20528/>

### Article

**Citation** (please note it is advisable to refer to the publisher's version if you intend to cite from this work)

**Ahuir Torres, JI, Kotadia, HR and Opoz, TT (2023) Effect of the electrical discharge machining on Ti6Al4V corrosion behaviour in simulated body fluid. Surface and Coatings Technology, 470. ISSN 0257-8972**

LJMU has developed [LJMU Research Online](#) for users to access the research output of the University more effectively. Copyright © and Moral Rights for the papers on this site are retained by the individual authors and/or other copyright owners. Users may download and/or print one copy of any article(s) in LJMU Research Online to facilitate their private study or for non-commercial research. You may not engage in further distribution of the material or use it for any profit-making activities or any commercial gain.

The version presented here may differ from the published version or from the version of the record. Please see the repository URL above for details on accessing the published version and note that access may require a subscription.

For more information please contact [researchonline@ljmu.ac.uk](mailto:researchonline@ljmu.ac.uk)

<http://researchonline.ljmu.ac.uk/>



## 25 1. Introduction

26 Titanium alloys, specifically Ti6Al4V, are widely employed as implant for the  
27 biomedical industry owing to the excellent properties as good corrosion resistance and  
28 excellent biointegrity [1-5]. The increasing life expectancy has, nevertheless, necessitated the  
29 need to extend the lifespan of implants to span several decades. The aggressive environment  
30 of the body fluid can corrode the Ti6Al4V at long-term. This can decrease the biointegrity  
31 and lifetime of this metallic material and produce the loosening of the implant after long-term  
32 [1, 4, 6]. The titanium dental implant can be corroded in saliva environment due to fluoride  
33 ions. Ti6Al4V passive film can be dissolved in the environment via the reaction of the  
34 fluoride ions that is highly chemical affinity to the titanium [5, 7]. Chloride, sulphate and  
35 phosphate ions of the blood can also react the passive film of Ti6Al4V, causing the breaking  
36 down the film and beginning the corrosion of the implant [4, 6, 8]. The breaking of the passive  
37 film is furthermore encouraged by the body temperature (37.5° C). The increase of the  
38 temperature accelerates the ion reactions with the passive film [4, 9]. In addition to the loss of  
39 the implant, the corrosion of Ti6Al4V can provoke other health problems because of the  
40 alloying elements. Aluminium is associated to the Alzheimer while vanadium is cytotoxic [3,  
41 10]. Thus, the increment of the corrosion resistance is an essential to improve the Ti6Al4V  
42 capacities as implants.

43 The corrosion resistance of the titanium alloy can be improved using varying  
44 techniques including, anodising [11, 12], plasma electrolytic oxidation [13], electrical  
45 discharge machining (EDM) [1, 14-17], ion implantation [18], sol-gel coatings [19], laser  
46 alloying [2], laser selective melting [20], thermal treatment [8], physical vapour deposition  
47 [21] and chemical vapour deposition [22]. EDM enhanced the corrosion resistance of the Ti  
48 alloy by generating layers with high chemical inactivity and good adhesion on the substrate  
49 [1]. The characteristics of the layers are dependent on the specific EDM conditions and type  
50 of the bath used. In non-aggressive environments, EDM induces microstructural changes in  
51 the titanium alloy, resulting in the formation of a new layer with high corrosion resistance  
52 [17]. When EDM is performed in a water bath, a thick passive film is produced on the  
53 metallic alloy, thereby increasing its corrosion resistance [16]. In the case of the EDM in  
54 hydroxyapatite dissolution bath, in addition to the thick passive film, a hydroxyapatite layer  
55 can be generated on the substrate through particle electrical deposition. This deposited layer  
56 exhibits excellent compaction and adhesion, providing protection for the metallic alloy  
57 against aggressive environments [1, 15]. Although similar effects were found in machined  
58 alloys with bath with carbon nanotubes [2], the hydroxyapatite layer possesses the benefit of  
59 increasing the material biocompatibility [14]. However, it is important to note that despite the  
60 corrosion resistance improvement achieved through EDM on Ti6Al4V, the process can also  
61 introduce cracks and pores. These imperfections can increase the titanium alloy's  
62 susceptibility to corrosion [23, 24]. The occurrence of these imperfections is influenced by the  
63 specific EDM conditions, such as capacitance and bath type [25, 26].

64 EDM technique furthermore is one of most suitable techniques to machine high  
65 strength and low thermal conductive materials. EDM is a non-contact machining method that  
66 utilizes a series of controlled electrical sparks between the workpiece and an electrode to  
67 erode the material. EDM offers several advantages for Ti alloy machining, including the  
68 ability to achieve intricate shapes, precise tolerances, and excellent surface finishes.

69 Additionally, EDM is a relatively low-temperature process, which helps to minimize the risk  
70 of thermal damage or distortion to the titanium alloy workpiece. In the context of bioimplant  
71 applications, the EDM technique enhances biocompatibility and promotes the desired surface  
72 roughness, facilitating improved wettability, hydrophilicity (allowing bone cells to adhere to  
73 the surface), proliferation, and anchorage [27-32].

74 The influence of EDM conditions on the corrosion resistance of machined Ti6Al4V in  
75 body fluid has been inadequately examined in the existing literature. Therefore, this study  
76 aims to investigate the corrosion resistance of Ti6Al4V machined through EDM under  
77 varying capacitance and bath conditions in simulated body fluid (SBF). The machining  
78 process was conducted using capacitances of 10nF, 100nF, and 500nF, and baths consisting of  
79 oil, water, and hydroxyapatite dissolution (HA). The surfaces and cross-sections of the  
80 samples were analysed using optical light profilometry and scanning electron microscopy,  
81 while the chemical composition was assessed using energy dispersive spectroscopy. The  
82 corrosion resistance and corrosion mechanism were evaluated through various  
83 electrochemical corrosion analyses, including potentiodynamic polarization curves (PPC) and  
84 electrochemical impedance spectroscopy (EIS) before and after the PPC test.

## 85 **2. Experimental Setup**

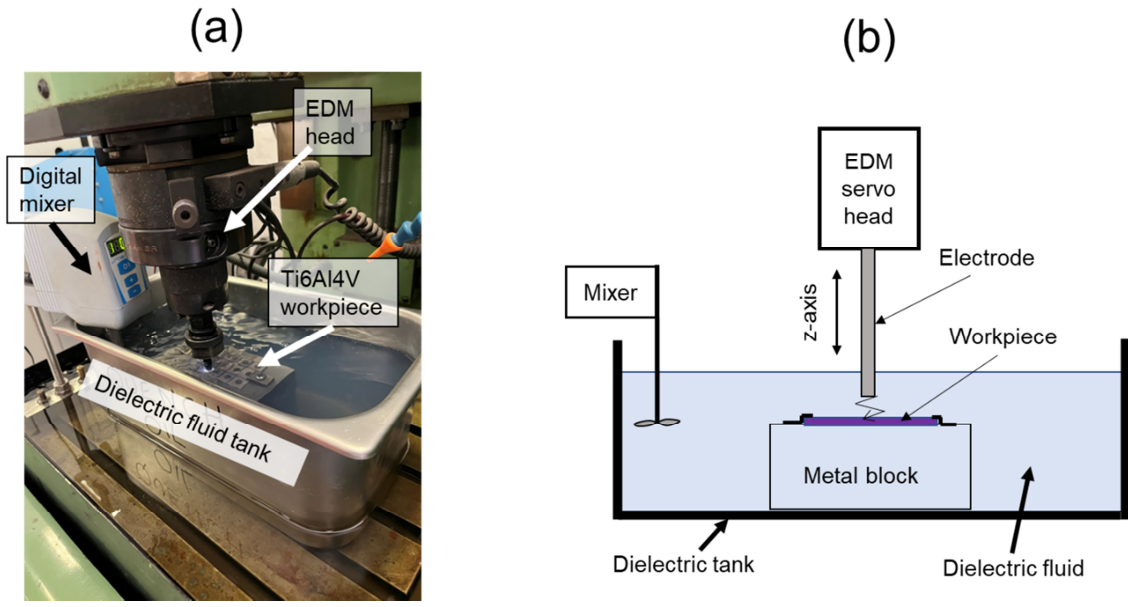
### 86 **2.1. *Materials and Electrical Discharge Machining***

87 In this study, a Ti-6 wt.% Al-4 wt.% V alloy was used as the workpiece material in the  
88 form of a 3 mm thick sheet. The sheet was cut into a small rectangular piece measuring 55x80  
89 mm. The experiments were conducted using a Hurco 50A Mark 2 die sinking type EDM  
90 machine.

91 For the electrode material, a solid circular graphite with a diameter of 6 mm was  
92 employed. To perform the EDM experiments under different dielectric conditions, a small  
93 dielectric reservoir was utilised, and the dielectric circulation system of the EDM machine  
94 was disconnected. The experimental setup is shown in **Fig. 1**.

95 Three different dielectric fluid conditions were employed in the experiment: EDM oil,  
96 deionized water, and a HA in deionized water. Hydroxyapatite powder, provided by Medicoat  
97 SAS based in France, with particle sizes ranging from 10 to 15  $\mu\text{m}$  was mixed with deionized  
98 water at a concentration of 10 g/L. A digital mixer was used to stir the dielectric fluid,  
99 preventing precipitation of hydroxyapatite powder and accumulation of debris and HA  
100 particles in the machining zone.

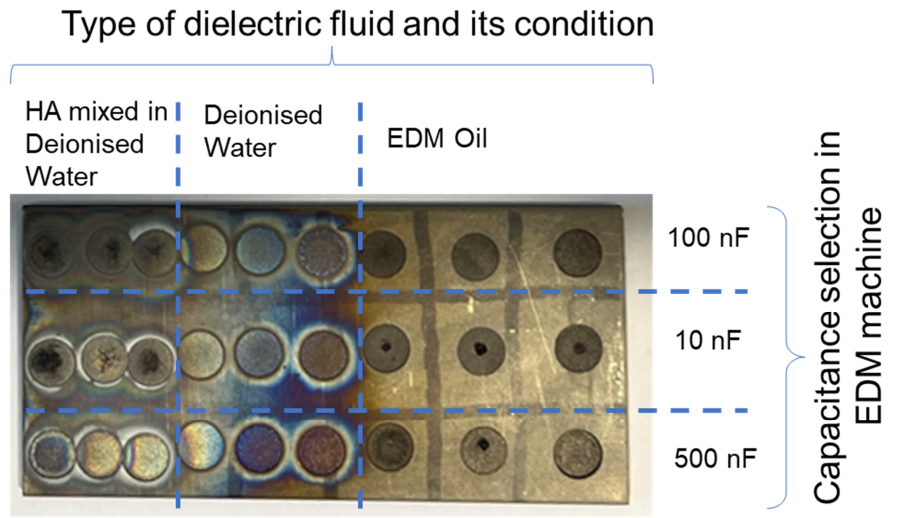
101 The EDM machine's capacitance was set at three different values: 10nF, 100nF, and  
102 500nF. A summary of the experimental parameters is presented in **Table 1**. **Fig. 2** illustrates  
103 the surfaces generated using EDM, consisting of 27 circular surfaces created under various  
104 dielectric fluid and capacitance settings. Each test was repeated three times to ensure the  
105 repeatability of the experiments.



106  
107 **Figure 1.** EDM machining setup (a) EDM set-up, (b) a schematic drawing of the  
108 experimental setup.

109 **Table 1.** Summary of EDM parameters used for the experiments.

Parameter	Description/Values
EDM machine	Hurco 50A Mark 2
Workpiece material	Ti6Al4V
Electrode	Solid circular graphite (6 mm in dia.)
Dielectric fluid	<ul style="list-style-type: none"> <li>Fully Synthetic Dielectric Oil (Corsmot EDM/CH PLUS)</li> <li>Deionised water,</li> <li>HA mixed in deionised water (10g/L HA concentration)</li> </ul>
Pulse time ( $\mu$ s)	20
Duty cycle (%)	50
Capacitance (nF)	10, 100, 500
Polarity (electrode)	Negative



110  
111 **Figure 2.** Macrostructures of EDMed Ti6Al4V workpiece material under different conditions.

112 **2.2. Electrochemical Analyses**

113 The non-electrical discharge machined (non-EDMed) samples also were polished with  
 114 1200p silicon carbide abrasive paper. All samples were cleaned after electrochemical analyses  
 115 with commercial detergent and fresh water soaking, then with distilled water rinsing and the  
 116 last cleaning step was isopropanol spray and drying with drier. The aggressive environment  
 117 was SBF formed of the next chemical compounds summarised in **Table 2** [6, 12, 33].

118 **Table 2.** SBF chemical compounds in g/L [6, 12, 33].

Chemical compound	Quantity (g per litre distilled water)
NaCl	8.035
NaHCO <sub>3</sub>	0.355
KCl	0.225
K <sub>2</sub> HPO <sub>4</sub> .3H <sub>2</sub> O	0.231
MgCl <sub>2</sub> .H <sub>2</sub> O	0.311
CaCl <sub>2</sub> .H <sub>2</sub> O	0.292
Na <sub>2</sub> SO <sub>4</sub>	0.072
((CH <sub>2</sub> OH) <sub>3</sub> (CNH <sub>2</sub> ))	6.118
pH	7.4

119

120 The chemical products used were provided by Merck. The pH of the SBF environment  
 121 was adjusted using 1 M HCl, and the pH measurements were taken using a pH meter (Jenway  
 122 350pH Meter) supplied by Scientific Laboratory Supplies. The temperature of the SBF was  
 123 maintained at 315.5 K throughout the testing, achieved using a hot plate (Stuart, SB162)  
 124 provided by BioCote.

125 The electrochemical experiments were conducted using a potentio/galvanostat  
 126 (Interface1010E) from Gamry Instruments Inc. The potentio/galvanostat was handled with  
 127 *Gamry Framework* software and the data were evaluated by mean of the *Gamry Echem*  
 128 *Analyst* software. The three-electrode cell was employed to carry out the electrochemical  
 129 analyses. The cell was consisted of a reference, counter and working electrode. The reference  
 130 electrode was silver/silver chloride in 3 M KCl (Ag/AgCl 3 M KCl) with double junction,  
 131 being supplied by EDT direct ion limited. The counter electrode was a platinum wire of 0.7  
 132 mm diameter that was provided by Cooksonglod Heimerle + Meule Group. The working  
 133 electrodes were the samples. The electrochemical testing was perturbative of direct current  
 134 (PPC) and of alternating current (EIS). PPC and EIS specifications were summarised in **Table**  
 135 **3.**

136 **Table 3.** Selected PPC specifications and EIS set up parameters.

Technique	Parameter	Value
PPC	Open circuit potential time	15 min
	Initial potential	Open circuit potential – 0.3 V
	Final potential	2.0 V vs Ag/AgCl 3M KCl
	Potential rate	0.167 mV/s
EIS	Potential amplitude in root mean square	10 mV
	Frequency range	Form 0.01 Hz to 100000 Hz
	Number of point per frequency decade	10

137

138 The samples were analysed with the next sequence of the techniques: EIS, PPC and  
139 EIS. The first EIS was made to study the corrosion mechanism of the non-polarised samples  
140 whilst the second EIS was conducted to understand the corrosion process of the samples  
141 polarised with PPC. The equivalent circuit method was utilised to assess the EIS data. *Gamry*  
142 *Echem Analyst* software was employed to develop the equivalent circuit method. All  
143 individual tests were repeated a minimum of three times to ensure the accuracy and reliability  
144 of the data.

### 145 **2.3. Surface and Microstructure Analysis Methods**

146 The EDM surfaces were analysed before and after the corrosion process using various  
147 microscopy techniques. Surface topography and roughness analyses of the EDM surfaces  
148 were performed using a Bruker Contour GT-K 3D white light interferometer equipped with  
149 *Vision 64* software (Optical light profilometer). The average areal surface roughness ( $S_a$ )  
150 values were used to compare the surface roughness of EDM surfaces under different dielectric  
151 fluid conditions and capacitance settings.

152 The surface characteristics and chemical composition of the samples were analysed  
153 using Scanning Electron Microscopy (SEM) with Energy Dispersive Spectroscopy (EDS).  
154 The SEM analysis was conducted at 10 kV with an 8.0 nA current and a 2.0 spot size. To  
155 prepare the samples for SEM analysis, standard Buehler grinding methodology was  
156 employed, followed by polishing using up to 0.05  $\mu\text{m}$ . After polishing, the samples were  
157 subjected to a 2-hour treatment with VibroMet<sup>TM</sup> using a silica suspension liquid.

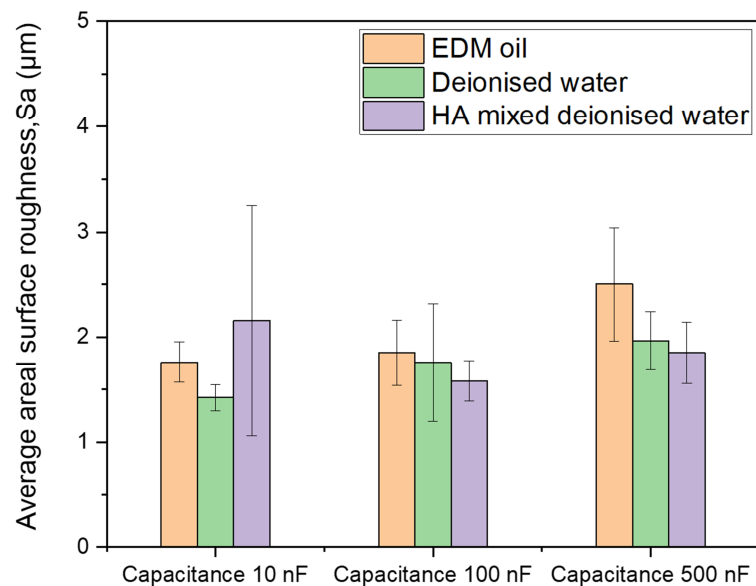
## 158 **3. Results**

### 159 **3.1. Surface and Microstructure Analyses after EDM**

160 **Fig. 3** illustrates the experimental results of surface roughness for different capacitance values  
161 (10nF, 100nF, and 500nF) and dielectric conditions (EDM oil, deionized water, and HA in  
162 deionized water). The surfaces machined in EDM oil exhibited higher surface roughness  
163 compared to those machined in deionized water, regardless of the capacitance values. The  
164 surface roughness values demonstrated an increasing trend with the rise in capacitance from  
165 10nF to 500nF, for both dielectric fluids, EDM oil, and water. The heightened capacitance led  
166 to an elevation in the heat energy produced per spark in the EDM system, resulting in the  
167 creation of larger craters on the surface of the workpiece. This effect was particularly  
168 significant due to the occurrence of multiple sparks throughout the EDM erosion process. It  
169 was not possible to observe individual crater formation due to a single spark. Consequently,  
170 numerous craters were formed on the machined surface, contributing to the roughness of the  
171 EDMed surfaces. The surface roughness of the surfaces machined in HA mixed in deionized  
172 water did not exhibit a consistent increasing or decreasing trend with varying capacitance  
173 values. Among the different capacitance values, the surfaces machined with a capacitance of  
174 10nF and HA mixed deionized water showed the highest surface roughness values. This can  
175 be attributed, in part, to the presence of HA powder causing unstable discharging and the low  
176 discharge energy not generating a strong pumping effect to remove debris particles in the  
177 discharging zone. The accumulation of debris particles and HA powder disrupted the  
178 discharging mechanism, resulting in higher surface roughness with a high standard deviation

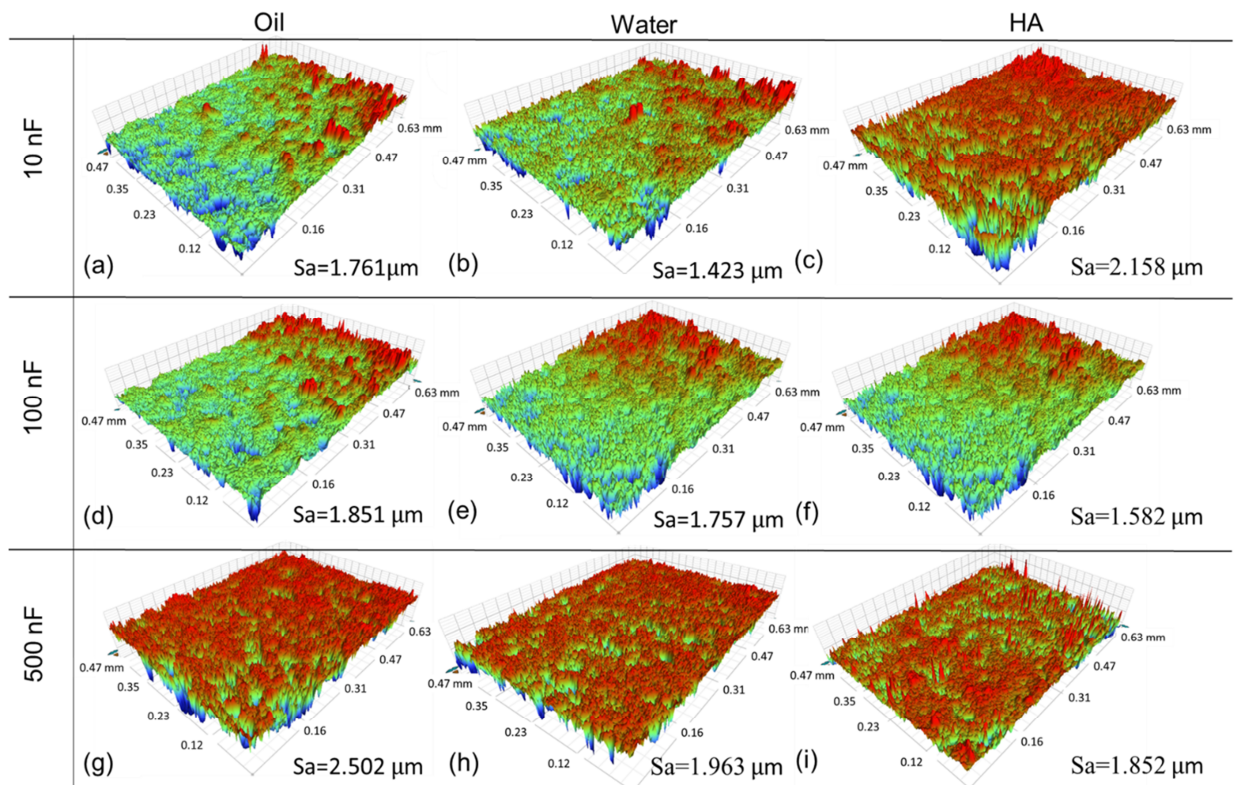
179 of 1.094 at 10nF capacitance. In contrast, the standard deviations of surface roughness  
180 obtained with EDM oil and deionized water at 10nF capacitance were 0.191 and 0.126,  
181 respectively, indicating more stable and repeatable results.

182 Higher capacitance values allowed the discharge mechanism to generate greater heat  
183 energy and stronger sparks, resulting in an adequate pumping effect that effectively expelled  
184 debris particles and HA powder from the machining region. This led to a more stable and  
185 predictable process. The standard deviations of surface roughness for the surfaces machined  
186 in HA mixed deionized water with capacitance values of 100 nF and 500 nF were 0.194 and  
187 0.290, respectively, indicating improved repeatability compared to the surfaces machined with  
188 a lower capacitance of 10nF. When considering larger capacitance values, such as 100nF and  
189 500nF, EDM with HA mixed deionized water demonstrated superior surface roughness  
190 compared to surfaces machined with EDM oil and water. This improved surface roughness  
191 can be attributed to the alteration of the discharge mechanism due to the inclusion of powder.  
192 The mechanism of powder mixed EDM has been extensively discussed in the literature [27],  
193 where smaller and more frequent discharges are generated in powder EDM. This leads to the  
194 formation of smaller craters with each discharge, ultimately resulting in reduced surface  
195 roughness compared to non-powder EDM processes.



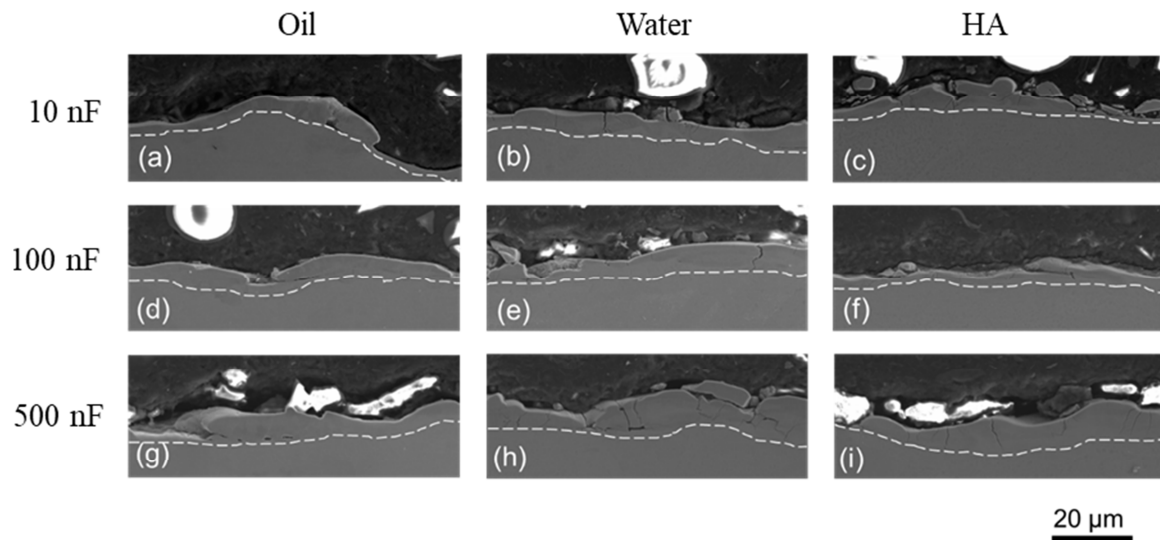
196  
197 **Figure 3.** Average areal surface roughness ( $S_a$ ) of the EDMed surfaces.

198 **Fig. 4** presents a supporting 3D surface topography obtained from the Bruker  
199 interferometer, where the red colour indicates the distribution of heights from the valley. As  
200 depicted in **Fig. 4**, the surfaces machined via EDM in oil and deionized water exhibit a  
201 significant increase in roughness as the capacitance values are raised. Additionally, the  
202 surfaces machined in EDM oil tend to have rougher surfaces compared to other surfaces  
203 except the surfaces machined with HA mixed deionized water with 10nF setting. However,  
204 surfaces machined with HA mixed deionized water demonstrate improved surface finish  
205 compared to both EDM oil and deionized water, except when the capacitance value was set to  
206 10nF.



207  
 208 **Figure 4.** Bruker 3D surface topography images of electric discharge machined (EDMed)  
 209 surfaces at different capacitance levels: (a-c) 10nF, (d-f) 100nF, and (g-i) 500nF. The images  
 210 show the surfaces before corrosion in (a), (d), and (g) oils, (b), (e), and (h) distilled water, and  
 211 (c), (f), and (i) a bath containing a mixture of hydroxyapatite and distilled water.

212 **Fig. 5** illustrates the SEM images of cross-sectional view of EDMed samples.  
 213 Typically, cross-sectional analysis is conducted in EDM-related research to examine the  
 214 characteristics of the white layer (molten layer) including hardness, crack formation, heat-  
 215 affected zone, and its thickness. However, in this study, the focus is on identifying  
 216 characteristics such as cracks or different layer formations that might affect the corrosion  
 217 analysis. The resolidified layer (white layer) becomes thicker as the capacitance value  
 218 increases, which is directly related to the amount of energy applied to the surfaces. EDM  
 219 mechanisms with higher capacitance values generate more significant heat energy, resulting  
 220 in a thicker resolidified layer. While electrical discharge machining with EDM oil does not  
 221 produce many cracks on the sub-surfaces, machining with deionized water and HA mixed  
 222 deionized water leads to the formation of several cracks on the resolidified layer. The cracks  
 223 formed with deionized water alone are larger and more prominent compared to the cracks  
 224 formed with HA mixed deionized water. The oil EDM sample exhibits voids and holes on the  
 225 machined area. The impacts of these characteristics on the corrosion analysis will be  
 226 discussed in the subsequent section.



227

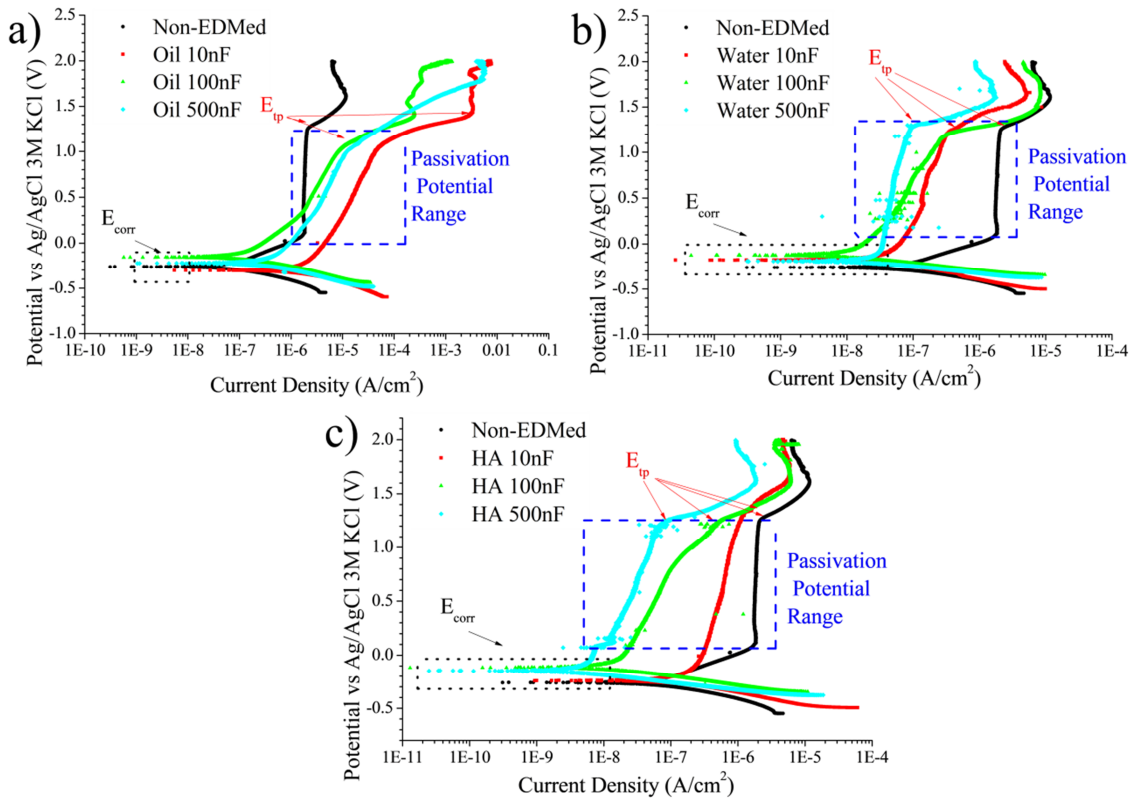
228 **Figure 5.** SEM images of cross-sectional view of non-corroded EDMed surfaces at (a-c)  
 229 10nF, (d-f) 100nF and (g-i) 500nF in (a), (d) and (g) oil, (b), (e) and (h) deionised water  
 230 (water) and (c), (f) and (i) HA mixed with distilled bath (HA), where the dotted white line  
 231 indicates the presence of the white layer (molten layer).

232 **3.2. Electrochemical Assessments**

233 **3.2.1. Potentiodynamic Polarisation Curves, Direct Current.**

234 All samples were subjected to testing using SBF to generate the potentiodynamic  
 235 polarization curve. **Fig. 6** illustrates the resulting PPC curve obtained from all samples. As  
 236 shown in **Fig. 6**, the potentiodynamic polarization curves exhibited a similar shape.

237 The reduction or cathodic branch of the curve appeared as a horizontal line, indicating  
 238 that the cathodic reaction is primarily controlled by activation [34]. On the other hand, the  
 239 anodic or oxidation branch of the curve displayed a vertical shape at low potential, indicating  
 240 the presence of a passive film on the samples [12, 34]. At high potential, the curve exhibited a  
 241 slight incline, indicating the occurrence of transpassivation of titanium dioxide ( $\text{TiO}_2$  [12])  
 242 which transforms into other oxide forms such as  $\text{TiO}_4$  or non-stoichiometric oxides. These  
 243 oxidised forms also possess a protective/passive nature [5, 35, 36] as indicated by the vertical  
 244 shape of the curve at the highest potential. The potential at which the transition from  
 245 passivation to transpassivation occurs is often referred to as the transpassivation potential ( $E_{tp}$ )  
 246 [35]. Some samples (EDMed samples at 100nF and 500nF in water and HA bath) exhibited  
 247 current fluctuations in the cathodic branch, indicating the generation of metastable  
 248 micropitting [35, 36].



249

250

251 **Figure 6.** PPC of non-machined (non-EDMed) and electrical discharge machined Ti6Al4V at  
 252 10 nF, 100 nF and 500 nF with (a) oil, (b) distilled water (water) and (c) hydroxyapatite  
 253 dissolution (HA) in SBF immersion at 7.4 pH and 313 K.

254

255

256

257

258

259

260

261

262

263

264

265

266

267

268

269

270

271

272

273

274

The corrosion characteristics of the samples, such as corrosion potential, corrosion rate, passivation potential range and passivation rate, polarization resistance, and transpassivation potential, varied among the different samples (**Fig. 7**). These features were determined based on the data obtained from the PPC. The majority of the machined samples had higher corrosion potential ( $E_{corr}$ ) than that for non-EDMed samples (**Fig. 7(a)**). The oxidised layer generated during EDM is nobler than native passive film. The electrical discharges activate the metal to react with the aggressive environment, producing a compact oxidised layer [15]. The only exception was the samples machined at 10nF and oil bath where  $E_{corr}$  was lower than non-EDMed samples. The low capacitance and aggressiveness of the environment hinder the completed oxidised layer formation. The imperfections as cracks, cavities and inhomogeneity can also decrease the nobility of the metallic materials [37].  $E_{corr}$  of the samples produced in more aggressive environment (water and hydroxyapatite dissolution) was higher than less harsh environment (oil bath). The oxidative environment produces oxidised layer thicker than the layers created in less harsh bath. The nobility of the oxide layer is proportional to the thickness and homogeneity [38]. In respect of the capacitance, EDMed Ti6Al4V samples created at 100nF had higher  $E_{corr}$  for water and HA baths. The thickness and homogeneity of the oxide layer also is proportional to capacitance [1]. An excessive capacitance can produce imperfections (e.g., cracks and pores) and other oxidised forms that diminishes the nobility of the alloy [2, 23].

The corrosion rate ( $C.R._{corr}$ ) of the samples can be observed in **Fig.7(b)** and these were estimated using equation (1) [2, 16, 39, 40].

$$C.R._{corr} = \frac{I_{corr} * M}{\rho * F * n} \quad (1)$$

Where,  $I_{corr}$  is the corrosion current density,  $M$  is the titanium molar mass (47.867 g/mol [41]),  $\rho$  is the Ti6Al4V density (4.43 g/cm<sup>3</sup> [42]),  $F$  is the Faraday's constant (96500 coulombs per mole (C/mol) [43]) and  $n$  is the electron number transferred in the corrosion reaction (4 electrons [41]).  $I_{corr}$  was estimated with the intersection of the cathodic and anodic Tafel linear regression [3, 44]. The choice of this particular corrosion feature was based on its ability to provide a more visually tangible representation of the corrosion kinetics. The majority of the machined samples had lower  $C.R._{corr}$  than non-machined samples. The oxidised layer formed during EDM is compact and protective, being a passive film [36, 40]. The chemical inactivity of the passive film commonly is proportional to its thickness [1]. Note that the samples machined in hydroxyapatite dissolution bath, the deposition of the hydroxyapatite on surface can create an extra protective film [1]. Only exceptions were EDMed samples in oil bath herein only the samples machined at 500nF possessed slower  $C.R._{corr}$  than non-machined samples. EDMed samples produced in oil bath at 10nF possessed higher  $C.R._{corr}$  while that for the samples machined at 100nF,  $C.R._{corr}$  was similar to non-EDMed sample  $C.R._{corr}$ . This means that the generation and thickness of the EDMed oxidised layer is encouraged with the increasing of the capacitance. These oxidised layer features define the corrosion rate of the samples. The capacitance used in EDM also had an influence on the corrosion rate ( $C.R._{corr}$ ) of the samples fabricated in water and hydroxyapatite bath. For the samples machined in water, the  $C.R._{corr}$  followed the order of 10nF > 500nF > 100nF. Lower capacitance values resulted in the formation of a thinner oxidised layer, while higher capacitance values led to the creation of cracks and imperfections that increased the susceptibility to corrosion [23]. On the other hand, for the samples produced in the hydroxyapatite dissolution bath, increasing the capacitance decreased the  $C.R._{corr}$ . This was attributed to the thicker hydroxyapatite layer formed on the surface at higher capacitance levels, as the capacitance promoted the deposition of hydroxyapatite on the Ti6Al4V material. The hydroxyapatite layer also exhibited a protective effect [1, 23]. It should be noted that the  $C.R._{corr}$  of the EDMed samples could be lower due to the larger contact area between the aggressive environment and the metallic alloys caused by the higher average surface roughness [45].

The polarisation resistance ( $R_p$ ) of the samples can be seen in **Fig.7(c)** and was estimated using the equation (2) [39, 46-48].

$$R_p = \frac{\beta_a * \beta_c}{2.303 * I_{corr} * (\beta_a + \beta_c)} \quad (2)$$

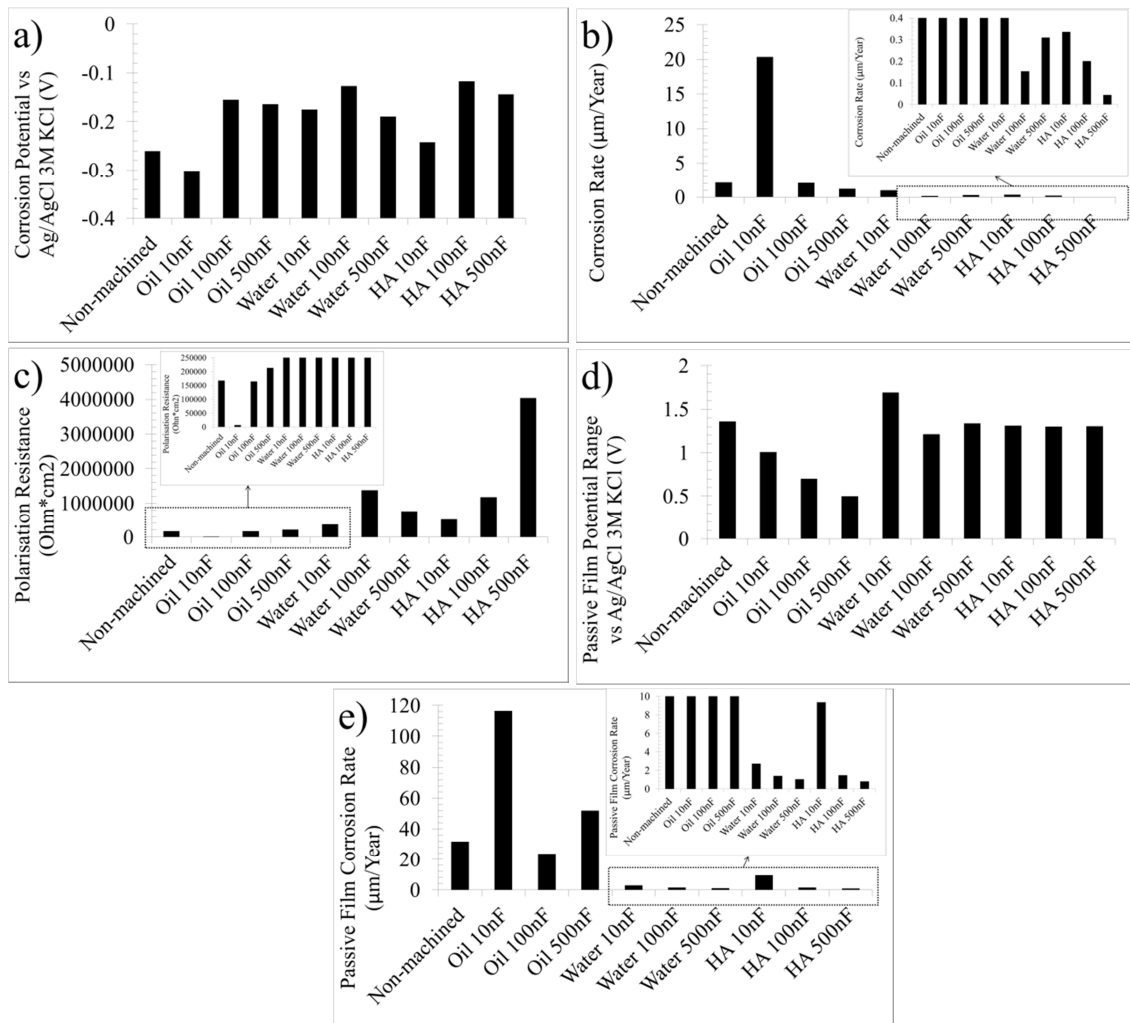
The anodic and cathodic slopes, denoted as  $\beta_a$  and  $\beta_c$ , respectively, exhibited contrasting trends compared to  $I_{corr}$  with respect to the electrical discharge machining parameters. This behaviour is expected since  $R_p$  (polarization resistance) and  $I_{corr}$  (corrosion current) are inversely proportional to each other [39, 46-48].

The passive film potential range (**Fig.7(d)**) was the substitution of  $E_{tp}$  with  $E_{corr}$ . The samples machined in oil bath had lower passive film potential range than that for non-machined samples, indicating that the passive film of the samples machined in oil bath was less thermodynamic stable than the native passive film. Chang-bing et al. [32] noted that the titanium carbide formed during EDM process is less stable than pure oxide titanium layer for

317 SBF. The passive film range was reduced with the increment of the capacitance for the silicon  
318 oil bath. The cracks and the roughness decrease the stability of the passive film [45]. In the  
319 other bath, EDMed samples showed similar passive film potential range for each other and to  
320 non-EDMed samples.

321 The passive film corrosion rate was calculated using the equation (1), where  $I_{corr}$  was  
322 replaced by passive film current density that was defined how current density of the passive  
323 film potential range. Note that this is the predominant parameter in the corrosion kinetic for  
324 the passive materials. This parameter was dissimilar according to the EDM conditions  
325 (**Fig.7(d)**). The samples machined in the oil bath exhibited a higher corrosion rate of the  
326 passive film compared to the non-machined sample, indicating lower corrosion resistance.  
327 However, the sample machined at 100nF showed a similar corrosion rate to the non-EDMed  
328 samples, deviating from the trend. As previously explained, this can be attributed to the  
329 formation of a thin oxidised layer in the 10nF samples and the presence of a high number of  
330 imperfections in the 500nF samples. On the other hand, the samples machined in water and  
331 hydroxyapatite dissolution bath displayed a lower corrosion rate of the passive film compared  
332 to the non-machined samples. This can be attributed to the lower electrical conductivity of the  
333 passive film formed in the presence of water compared to the native passive film [11].  
334 Furthermore, an increase in capacitance resulted in a reduction of the corrosion rate of the  
335 passive film in both cases. This can be attributed to the increased thickness of the passive  
336 film, which hinders electron transfer. Previous studies [26, 40] have also supported these  
337 findings.

338  
339  
340  
341  
342  
343  
344  
345  
346  
347  
348  
349  
350  
351  
352  
353  
354  
355



356

357

358

359

360

361

**Figure 7.** Graphs of the (a) corrosion potential, (b) corrosion current density, (c) polarisation resistance, (d) passivation potential range and (e) passivation film corrosion rate of the samples in SBF according to EDM conditions.

362

### 3.2.2. Electrochemical Impedance Spectroscopy, Alternating Current.

363

364

365

366

367

368

369

370

371

372

373

374

375

376

377

378

The EIS assessments of the non-machined and machined samples can be observed in **Fig. 8**. The equivalent circuit method, Bode and Nyquist plots were utilised to analyse the EIS data. EIS analyses showed that the samples had dissimilar corrosion mechanism. The non-EDMed sample before PPC exhibited a corrosion mechanism characterized by three distinct time constants. The first time constant was identified in the Bode plots, where the modulus impedance ( $Z_{mod}$ ) showed a horizontal curve at high frequency ( $F$ ) ranges (1000 Hz-100000 Hz), indicating the presence of a resistance component [49]. The second- and third-time constants were characterized by a rounded peak in the phase angle ( $\theta$ ) vs frequency ( $F$ ) plots (Bode plots) at medium and low frequencies (0.01 Hz-1000 Hz). The distinct slopes of the inclined curves in the  $Z_{mod}$  vs  $F$  Bode plots also indicated the presence of these time constants. Both time constants showed a significant overlap, as evidenced by the rounded peak shape in the  $\theta$  vs  $F$  Bode plots and the circular shape of the Nyquist plot [50]. These time constants were formed by a parallel combination of capacitance and resistance elements [50].

After the PPC, the non-machined sample exhibited a corrosion mechanism with a similar number and type of time constants, but the overlap between the second- and third-time constants was reduced. This can be observed in the significant difference in slopes of the

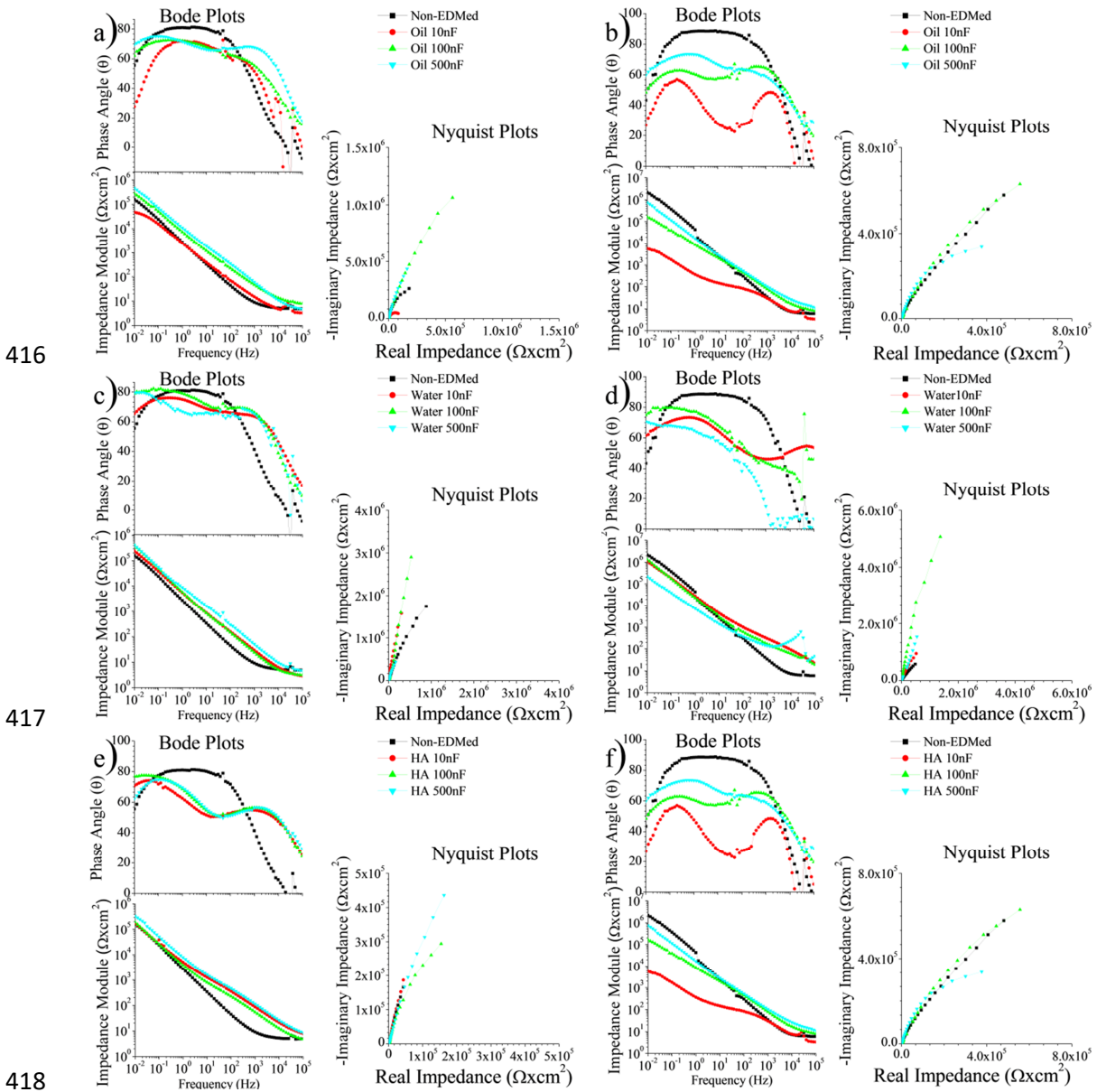
379 Bode plots ( $Z_{mod}$  vs  $F$ ). The reduction in overlap suggests changes in the characteristics of the  
380 passive film [6, 13, 51].

381 The Bode and Nyquist plots of the samples machined in oil bath before PPC (**Fig.8(a)**)  
382 had similar the corrosion mechanisms than the non-machined samples. The visible double  
383 peaks of the Bode plots ( $Z_{mod}$  vs  $F$ ) indicated the lower overlapping of second and third time  
384 constant. These signals were split in samples machined at higher capacity, meaning an  
385 increment of the microstructural change thickness with the increasing of the capacitance [52].  
386 The overlapping of the second and third time constants was lower after PPC (**Fig. 8(b)**),  
387 showing a chemical change or degradation of the surface [6, 13, 51].

388 For the EDMed samples in a water bath before PPC (**Fig. 8(c)**), the corrosion  
389 mechanisms exhibited similar characteristics to the samples machined in an oil bath. The only  
390 difference was observed in the EDMed samples at 500nF, showing a shift towards lower  
391 frequencies after the PPC. This shift may indicate a decrease in corrosion resistance due to  
392 passive film degradation [4].

393 The samples machined in a hydroxyapatite dissolution bath (**Fig.8(d)**) before PPC also  
394 exhibited a similar corrosion mechanism to the previous samples. These machined samples  
395 showed a comparable overlapping of the second and third constants after PPC, indicating that  
396 the hydroxyapatite layer and passive film remained intact after the corrosion process [5, 50].

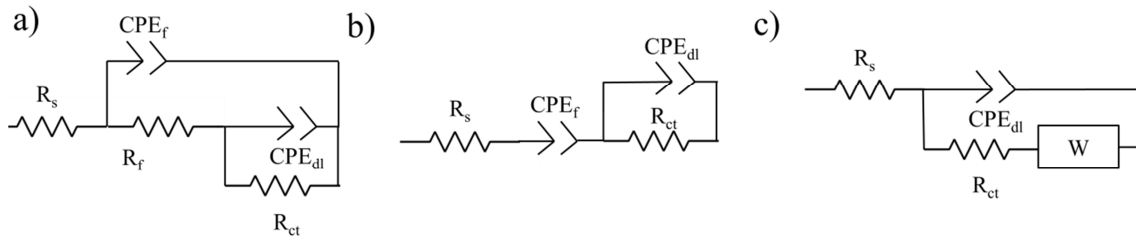
397  
398  
399  
400  
401  
402  
403  
404  
405  
406  
407  
408  
409  
410  
411  
412  
413  
414  
415



416  
417  
418  
419 **Figure 8.** Bode and Nyquist plots illustrating the comparison between non-machined and  
420 machined Ti6Al4V samples in different environments: EDMed (a) and (b) represent oil, (c)  
421 and (d) represent water, and (e) and (f) represent a hydroxyapatite dissolution bath in  
422 simulated body fluid (SBF) before (a), (c), and (e) and after (b), (d), and (f) potentiostatic  
423 pulse current (PPC) treatment.

424 The values of the corrosion processes in the corrosion mechanisms were calculated using an  
425 equivalent circuit simulation, which represents the corrosion process using elements of an  
426 electrical circuit [19, 36, 38]. Three circuits were employed to represent the corrosion  
427 mechanism of the samples (**Fig. 9**), indicating that the initial assumption based on  
428 experimental data was incorrect. The first circuit (**Fig.9(a)**) closely resembled the proposed  
429 circuit based on experimental data. The first-time constant represented the dissolution  
430 resistance ( $R_s$ ), and the second time constant represented the passive film ( $R_f$  and  $CPE_f$ ). Both  
431 elements were in series with  $R_s$ . The final time constant corresponded to the charge transfer  
432 resistance ( $R_{ct}$ ) and the charge double layer ( $CPE_{dl}$ ) [5, 20, 50, 53]. The second equivalent  
433 circuit (**Fig. 9(b)**) was similar to the previous circuit, but  $R_f$  was absent. The last equivalent

434 circuit was identical to the previous circuit, except that  $CPE_f$  was replaced by bounded  
435 Warburg impedance (**Fig.9(c)**) [35].



436  
437 **Figure 9.** Schematic drawing of the (a) first, (b) second and (c) third equivalent circuit  
438 proposed.

439 The simulated data (**Fig. 10**) showed a good agreement with the experimental data,  
440 and the low chi-square values (**Table 4**), ranging from  $10^{-4}$  to  $10^{-3}$ , confirmed the validity of  
441 the simulation results [19]. The first equivalent circuit was the most observed circuit,  
442 representing most of the samples. The second circuit was found for the electrical discharge  
443 machined samples in water at 10nF before and after PPC, as well as in hydroxyapatite at 10nF  
444 before PPC. The third equivalent circuit represented the EDMed sample at 100nF in water and  
445 hydroxyapatite after PPC. The transpassivation process resulted in the formation of  
446 imperfections in the passive film, such as surface pitting and cracks, which influenced the  
447 diffusion processes within the film [36, 54].

448

449

450

451

452

453

454

455

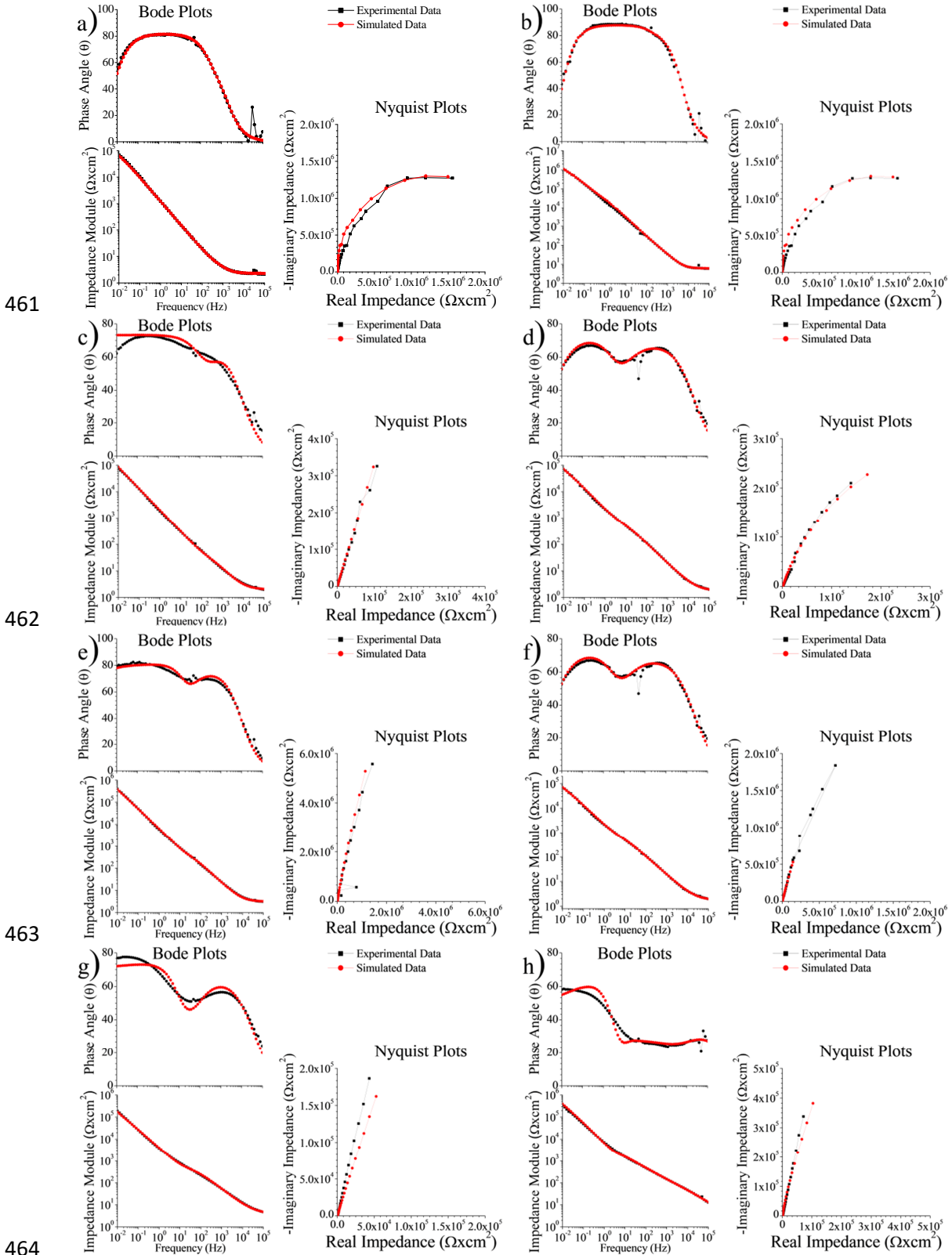
456

457

458

459

460



461  
462  
463  
464  
465 **Figure 10.** Comparison of the Bode and Nyquist plots between experimental and simulated  
466 data of the (a) and (b) non-machined and (c-h) machined at 10nF in oil c-d), water e-f) and  
467 hydroxyapatite dissolution g-h) bath for SBF immersion at 315K and 7.4pH.

468 **Table 4** presents a summary of the values of the equivalent circuit elements. The  
469 values of  $R_S$  for all samples ranged from  $2 \Omega \times \text{cm}^2$  to  $7 \Omega \times \text{cm}^2$  indicating their dependency  
470 solely on the dissolution process [45, 49].

471 After PPC, there were notable changes in the other elements of the equivalent circuit.  
472 For the non-EDMed Ti6Al4V samples,  $R_f$  decreased while  $CPE_f$  increased, indicating that the  
473 protective capacity of the transpassivation passive film was lower compared to the original  
474 passive film. The value of  $n_f$  decreased from 1.00 to 0.90 after PPC, suggesting the presence  
475 of imperfections in the transpassivation film [4, 5, 20, 45]. On the contrary,  $R_{ct}$  increased after  
476 PPC, and  $CPE_{dl}$  decreased, indicating an improvement in the corrosion resistance of the  
477 exposed material. The value of  $n_{dl}$  remained at 0.85 after PPC, suggesting that the surface  
478 topography remained rough below the passive film [4, 5, 20, 45].

479 In contrast, the EDMed samples in the oil bath at 10nF and 100nF exhibited an  
480 opposite behaviour, indicating that the transpassivation process enhanced the corrosion  
481 resistance of the passive film. As for the EDMed samples in the HA dissolution bath, most of  
482 the equivalent circuit element values remained unchanged before and after PPC, indicating  
483 that the passive film formed in this process remained similar properties after transpassivation.  
484 After PPC treatment, the values of  $n_f$  and  $n_{dl}$  exhibited lower values, suggesting alterations in  
485 the material topography. However, these changes had minimal impact on the corrosion  
486 properties. Similar trends were observed for the EDMed samples in the water bath at 10nF,  
487 where  $R_{ct}$  increased,  $CPE_f$  and  $CPE_{dl}$  decreased after PPC, suggesting an increase in the  
488 chemical inactivity of the passive film. The values of  $n_f$  and  $n_{dl}$  remained similar before and  
489 after PPC. Similar evolution of the passive film was also observed in the EDMed samples in  
490 the oil and water baths at 500nF.

**Table 4.** The equivalent circuit element values for the non-machined and EDMed Ti6Al4V

Sample	PPC	$R_s$ ( $\Omega\text{cm}^2$ )	$R_f$ ( $\text{k}\Omega\text{cm}^2$ )	$\text{CPE}_f$ ( $\mu\text{S}/\text{s}\text{cm}^2$ )	$n_f$	$R_{ct}$ ( $\text{k}\Omega\text{cm}^2$ )	$\text{CPE}_{dl}$ ( $\mu\text{S}/\text{s}\text{cm}^2$ )	$n_d$	$W$ ( $\mu\text{S}/\text{s}^{1/2}\text{cm}^2$ )	$n_w$	$X^2 (10^{-3})$
Non-machined	Before	6.131	2610.000	5.258	1.00	0.150	6106.782	0.85	-	-	0.987
	After	1.96	0.599	253.798	0.9	9510.000	9.510	0.85	-	-	1.043
Oil 10nF	Before	4.021	0.159	37.210	0.87	117.716	26.362	0.93	-	-	0.525
	After	5.017	249.788	40.298	0.76	15.893	133.690	0.93	-	-	0.374
Oil 100nF	Before	7.802	0.307	18.500	0.80	1540.000	96.200	0.84	-	-	1.640
	After	6.866	6.040	16.500	0.76	846.000	10.400	0.86	-	-	1.480
Oil 500nF	Before	2.820	16.1710	63.948	0.75	20.401	130.252	0.82	-	-	1.570
	After	2.099	0.364	132.385	0.70	43.134	1.581	1.00	-	-	5.860
Water 10nF	Before	4.711	-	10.050	0.81	3.080	11.110	0.76	-	-	1.430
	After	6.486	-	4.740	0.82	0.618	3.703	0.72	-	-	0.701
Water 100nF	Before	2.919	0.240	111.748	0.76	2140.000	33.062	0.90	-	-	0.563
	After	3.778	-	-	-	0.011	124.078	0.80	45.900	0.98	0.563
Water 500nF	Before	5.180	1.563	8.277	0.89	1720.000	6.338	1.00	-	-	0.564
	After	3.905	0.265	12.621	0.80	1180.000	6.028	0.86	-	-	0.563
HA 10nF	Before	4.712	-	11.110	0.76	2.177	10.500	0.81	-	-	1.430
	After	2.960	0.589	250.580	0.50	9508.000	51.334	0.82	-	-	1.420
HA 100nF	Before	3.819	0.757	28.351	0.74	19014.534	27.035	0.90	-	-	1.920
	After	2.424	-	-	-	0.086	8.979	0.68	60.719	0.32	2.710
HA 500nF	Before	6.240	1.480	15.800	0.72	4530.973	12.000	0.89	-	-	4.370
	After	7.100	1.927	14.012	0.59	2312.139	21.221	0.79	-	-	1.360

### 3.3. Microstructure analysis after electrochemical test

The surface characteristics of the samples before and after PPC are shown in **Fig. 11**. The surfaces of the EDMed samples exhibited a similar appearance, indicating that the transpassivation process had only a minor effect on the surface topography. In contrast, the non-EDMed samples showed a darkened area after PPC, indicating the oxidation of the Ti6Al4V material. The occurrence of localized oxidations can be attributed to the transpassivation process [12, 38]. However, in the case of the EDMed samples, such darkened areas were not observed because the material had already undergone oxidation during the EDM process [25, 26].

After PPC, the cross-section of the EDMed samples exhibited an additional layer, being attributed to the deposition of dissolved salts. During the PPC process, a portion of the electrical current can be utilized to transfer ions, which are subsequently reduced and deposited onto the surface [38]. This deposited layer displayed a higher prevalence of cracks and pores. It is noteworthy that all samples exhibited cracks both before and after PPC, indicating that the transpassivation process did not significantly alter the internal structure of the Ti6Al4V material.

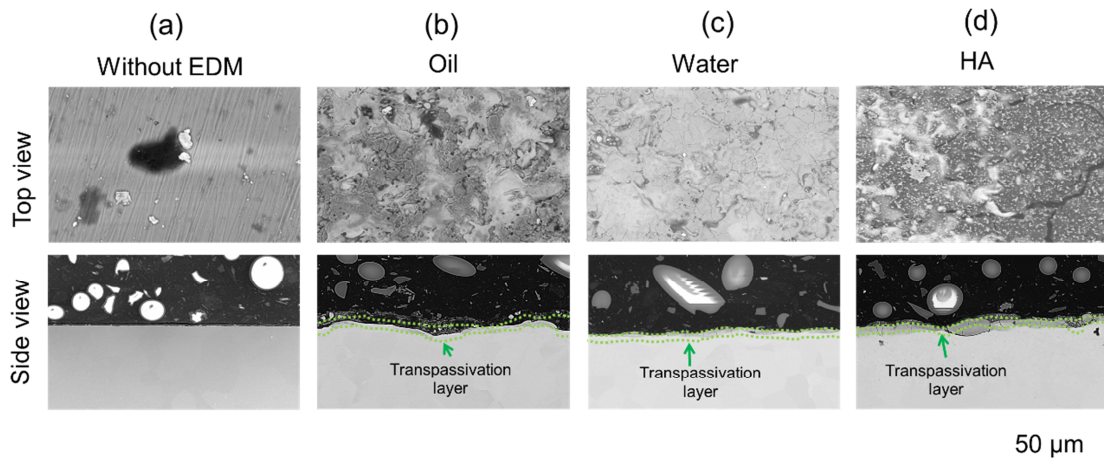
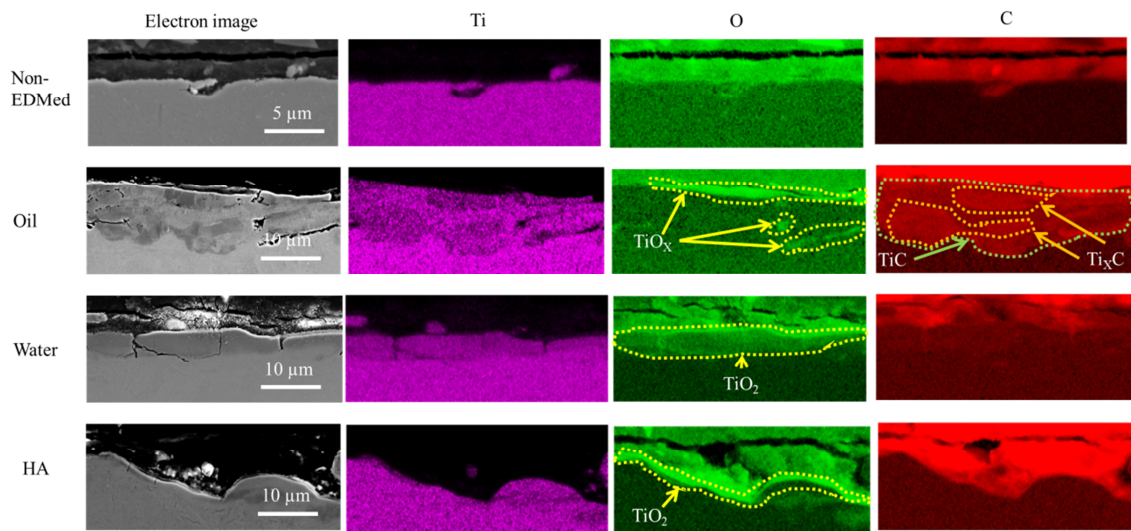


**Figure 11.** SEM micrograph of (a) non-EDMed (without EDMed) and samples EDMed (100nF) samples at (b) oil, (c) water and (d) HA bath (after PPC study).

The chemical composition maps of the sample cross sections focused on interested elements (titanium, oxygen and carbon) can be seen in **Fig. 12**. Non-EDMed specimens were mainly formed of titanium, indicating the passive film of this sample is thin. Oil bath samples had a low titanium concentration on the surface and localised zones with high oxygen and carbon concentration. Although the carbon was present on the surface, the concentration was dissimilar on the surface. These outcomes indicated that the surface chemical composition of these specimens was heterogeneous, which is a cause of their low corrosion resistance. Holsten et [55] observed that this is due to the cathodic (negative) polarisation of the tool hinders the carbon reaction with the Ti6Al4V and pure-Ti in oil bath. This causes a heterogeneous and thin titanium carbide layer. The researchers also observed that the samples EDMed in water bath had surface totally oxidised, indicating that this process only occur in oil bath. EDMed samples in

32 water and HA bath showed a high oxygen concentration on surface and low titanium  
 33 concentration. The presence of a thick passive film on these specimens has been  
 34 revealed by these results, indicating its formation during the EDM process, as  
 35 previously mentioned. EDMed samples in water bath possessed a passive film thicker  
 36 than the surface generated in HA dissolution in distilled water, which is a reason of the  
 37 better corrosion resistance of the water EDMed specimens as described before. In both  
 38 cases, the passive film was larger than non-EDMed specimens, providing their superior  
 39 corrosion resistance.

40 Notting EDS is infeasible to determine the chemical compound with exactitude  
 41 because this technique can only detect the elements and not the molecules.  $TiO_2$  and  
 42  $TiC$  however are the most common molecules when the oxygen concentration is high.  
 43 On other hand, the non-stoichiometric molecules ( $TiO_x$  and  $Ti_xC$ ) are the most usual  
 44 for low oxygen concentration. Aluminium and vanadium oxidise can be found these  
 45 zones.



46  
 47 **Figure 12.** EDS chemical composition maps of the 10nF samples after PPC study  
 48 where  $TiO_x$  is non-stoichiometric titanium oxide with oxygen deficient,  $TiO_2$  is titanium  
 49 dioxide,  $TiC_x$  is non-stoichiometric titanium carbide with carbon deficient and  $TiC$  is  
 50 titanium carbide.

#### 51 4 Discussion

52 The dissimilarity in corrosion resistance among the samples is attributed to the  
 53 formation of an oxide layer during EDM. Samples subjected to a less aggressive  
 54 environment, such as an oil bath and low capacitance, exhibited a heterogeneous and  
 55 thin oxidised layer. The charge transfer of the passive film was inversely proportional to  
 56 the thickness of the passive film [25, 26], resulting in an anodic effect on the non-  
 57 oxidised areas, thereby promoting corrosion [7]. Increasing the capacitance (500nF)  
 58 mitigated this effect; however, it led to the formation of cracks and a higher average  
 59 roughness, which consequently decreased corrosion resistance. The roughness  
 60 contributed to an increase in the exposed area and the presence of crevices [45], while

61 cracks further facilitated crevice corrosion [2]. Consequently, EDMed samples  
62 produced in an oil bath demonstrated lower corrosion resistance compared to non-  
63 EDMed samples.

64 The adverse effects of cracks and roughness on the corrosion surface were  
65 eliminated when the oxidised layer became homogeneous and thick. This condition was  
66 achieved in aggressive environments such as water and hydroxyapatite dissolution,  
67 coupled with high capacitance. The environment supplied oxidant elements that  
68 chemically activated the metallic alloy [15, 25] in conjunction with the capacitance [52].  
69 The presence of the oxidised layer even eliminated the detrimental effects of cracks,  
70 being typically caused by thermal stress [2]. As a result, EDMed samples fabricated in  
71 water and hydroxyapatite demonstrated higher corrosion resistance compared to non-  
72 EDMed samples. It is worth noting that hydroxyapatite EDMed samples exhibited  
73 lower corrosion resistance than water EDMed samples. The potential part of PPC,  
74 represented by the anodic branch passivation range, was utilized for depositing SBF  
75 ions onto the Ti6Al4V surface [38, 40]. The thickness of the oxidised layer can  
76 chemically be inactivated and is directly proportional to the EDM capacitance [26, 40].  
77 While the hydroxyapatite coating provides a protective effect, it is relatively weaker  
78 compared to the protection offered by the oxidised layer. The highest corrosion  
79 resistance was observed in EDMed samples produced at the highest capacitance, owing  
80 to the dependence of the corrosion resistance with the oxidised layer thickness.

81 The corrosion mechanisms observed in the Ti6Al4V samples were generally  
82 similar across all samples. These mechanisms consisted of a solution resistance, a  
83 passive film, and exposed materials. The passive film surfaces of the EDMed samples  
84 exhibited roughness, resulting in a surface roughness factor ( $n_f$ ) lower than 1, primarily  
85 due to the generation of pores on the outer layer [4, 5, 20, 45]. The presence of these  
86 similar corrosion mechanisms indicated that the presence of cracks and high average  
87 roughness had a minimal effect on the corrosion behaviour of EDMed Ti6Al4V, as the  
88 samples exhibited significant corrosion resistance.

89 The impact of transpassivation on corrosion resistance (as observed through  
90 EIS) varied among the samples. The microstructures of the samples remained  
91 unchanged after PPC. Transpassivation induced a chemical evolution of the passive  
92 film, leading to modifications in its chemical structure. This chemical evolution could  
93 differ based on the elements involved in the formation of the passive film, which in turn  
94 depended on the EDM parameters [36]. Notably, the influence of transpassivation on  
95 the corrosion resistance of samples immersed in a HA dissolution in distilled water bath  
96 was minimal, indicating the high stability of the passive film in this case [1, 50]. The  
97 additional layer formed during PPC through the electrodeposition of SBF salt had a  
98 negligible effect on corrosion resistance. The presence of a high number of defects, such  
99 as cracks and pores, in the deposited layer significantly reduced its protective  
100 capabilities [23].

101 **5 Conclusions**

102 Based on a comprehensive electrochemical and microstructural study, the  
103 corrosion characteristics of the Ti6Al4V alloy were investigated under different EDM  
104 conditions in simulated body fluid. The following conclusions can be drawn from this  
105 analysis:

106 The EDMed samples exhibited higher nobility compared to the non-EDMed  
107 samples, primarily attributed to the formation of an oxidised layer during the electrical  
108 discharge machining processes.

109 The corrosion resistance of samples machined using electrical discharge in  
110 aggressive baths (such as water and hydroxyapatite dissolution) is higher compared to  
111 non-EDMed samples. When EDM is performed in an oil bath, the corrosion resistance  
112 of the samples decreases due to the formation of a heterogeneous layer. Samples  
113 furthermore produced with high capacitance exhibit greater corrosion resistance than  
114 those EDMed at low capacitance.

115 The corrosion mechanism remains similar for all samples before PPC, but it  
116 diverges afterward. The chemical evolution resulting from transpassivation varies  
117 depending on the oxidised elements present in the passive film. Additionally, this  
118 process leads to the electrodeposition of SBF elements on Ti6Al4V samples.

119 Although EDM samples immersed in water exhibit the highest corrosion  
120 resistance, an additional beneficial property is the presence of a hydroxyapatite film on  
121 these samples, which contributes to good biointegrity.

122 This research provides a cost-effective and efficient method for generating  
123 Ti6Al4V surfaces that offer both high corrosion resistance and excellent biointegration.  
124 The implications of this work are significant, benefiting various industries, particularly  
125 the biomedical sector.

126 **Declaration of Competing Interest**

127 The authors have no conflicts of interest.

128 **Acknowledgement**

129 This work was partially supported by Liverpool John Moore University, Faculty of  
130 Engineering and Technology (FET) Pump Prime Awards 2021/22.

131 **References**

- 132 [1] P.S. Bains, M. Bahraminasab, S.S. Sidhu, G. Singh, Proceedings of the Institution of  
133 Mechanical Engineers, Part H: Journal of Engineering in Medicine, 234 (2020) 232-  
134 242.  
135 [2] G. Singh, T.R. Ablyaz, E.S. Shlykov, K.R. Muratov, A.S. Bhui, S.S. Sidhu,  
136 Micromachines, 11 (2020) 850.  
137 [3] I. Lavos-Valereto, S. Woly nec, I. Ramires, A.C. Guastaldi, I. Costa, Journal of  
138 Materials Science: Materials in Medicine, 15 (2004) 55-59.  
139 [4] V. Alves, R. Reis, I. Santos, D. Souza, T.d.F. Gonçalves, M. Pereira-da-Silva, A.  
140 Rossi, L. Da Silva, Corrosion Science, 51 (2009) 2473-2482.

- 141 [5] M. Hussein, A. Madhan Kumar, A.F. Abdelaal, M. Abdul Azeem, *Metallurgical and*  
142 *Materials Transactions A*, 52 (2021) 4299-4309.
- 143 [6] S. Tamilselvi, V. Raman, N. Rajendran, *Electrochimica Acta*, 52 (2006) 839-846.
- 144 [7] B. Sivakumar, S. Kumar, T.S. Narayanan, *Wear*, 270 (2011) 317-324.
- 145 [8] C.A.R. Maestro, M.C. Ferreira, A.H.S. Bueno, A.M. de Sousa Malafaia,  
146 *Engineering Journal*, 24 (2020) 185-193.
- 147 [9] R.W.-W. Hsu, C.-C. Yang, C.-A. Huang, Y.-S. Chen, *Materials Science and*  
148 *Engineering: A*, 380 (2004) 100-109.
- 149 [10] R. Luo, Z. Liu, F. Yan, Y. Kong, Y. Zhang, *Applied surface science*, 266 (2013)  
150 57-61.
- 151 [11] J. Lu, G. Wei, Y. Yu, X. Zhao, Y. Dai, *Int J Electrochem Sci*, 12 (2017) 2763-  
152 2776.
- 153 [12] H.R.A. Bidhendi, M. Pouranvari, *Metallurgical and Materials Engineering*, (2012).
- 154 [13] E. Matykina, R. Arrabal, B. Mingo, M. Mohedano, A. Pardo, M. Merino, *Surface*  
155 *and Coatings Technology*, 307 (2016) 1255-1264.
- 156 [14] C. Prakash, M. Uddin, *Surface and Coatings Technology*, 326 (2017) 134-145.
- 157 [15] M. Al-Amin, A.M. Abdul-Rani, M. Danish, S. Rubaiee, A.b. Mahfouz, H.M.  
158 Thompson, S. Ali, D.R. Unune, M.H. Sulaiman, *Materials*, 14 (2021) 3597.
- 159 [16] A. Mahajan, S. Devgan, S.S. Sidhu, *Surface and Coatings Technology*, 405 (2021)  
160 126583.
- 161 [17] S.K. Manderna, P. Katyal, M. Gupta, V. Singh, in: *IOP Conference Series:*  
162 *Materials Science and Engineering*, IOP Publishing, 2022, pp. 012067.
- 163 [18] D. Krupa, J. Baszkiewicz, B. Rajchel, A. Barcz, J. Sobczak, A. Biliński, T.  
164 Borowski, *Vacuum*, 81 (2007) 1310-1313.
- 165 [19] A.A. El Hadad, E. Peón, F.R. García-Galván, V. Barranco, J. Parra, A. Jiménez-  
166 Morales, J.C. Galván, *Materials*, 10 (2017) 94.
- 167 [20] X. Chen, Q. Liao, M. Gong, Q. Fu, *Metals*, 13 (2023) 192.
- 168 [21] M.A. Hussein, N. Ankah, A.M. Kumar, M.A. Azeem, S. Saravanan, A.A. Sorour,  
169 N. Al Aqeeli, *Ceramics International*, 46 (2020) 18573-18583.
- 170 [22] M. Kalisz, M. Grobelny, M. Zdrojek, M. Świniarski, J. Judek, *Thin Solid Films*,  
171 596 (2015) 101-110.
- 172 [23] H. Yaşar, B. Ekmekci, *Surface Topography: Metrology and Properties*, 9 (2021)  
173 015015.
- 174 [24] S. Sethy, R.K. Behera, J.P. Davim, J. Rana, *Journal of Manufacturing and*  
175 *Materials Processing*, 6 (2022) 96.
- 176 [25] A. Pramanik, A. Basak, G. Littlefair, S. Debnath, C. Prakash, M.A. Singh, D.  
177 Marla, R.K. Singh, *Heliyon*, 6 (2020) e05554.
- 178 [26] J.T. Philip, J. Mathew, B. Kuriachen, *Journal of Manufacturing Processes*, 64  
179 (2021) 1105-1142.
- 180 [27] N. Ekmekci, B. Ekmekci, *Materials and Manufacturing Processes*, 31 (2016) 1663-  
181 1670.
- 182 [28] O. Tahsin, H. Yasar, M. MURPHY, N. EKMEKÇİ, B. EKMEKÇİ, *International*  
183 *Journal of Advances in Engineering and Pure Sciences*, 31 (2018) 1-10.
- 184 [29] S.-L. Chen, M.-H. Lin, G.-X. Huang, C.-C. Wang, *Applied surface science*, 311  
185 (2014) 47-53.
- 186 [30] P. Harcuba, L. Bačáková, J. Stráský, M. Bačáková, K. Novotna, M. Janeček,  
187 *Journal of the mechanical behavior of biomedical materials*, 7 (2012) 96-105.
- 188 [31] F. Otsuka, Y. Kataoka, T. Miyazaki, *Dental materials journal*, 31 (2012) 309-315.
- 189 [32] T. Chang-bin, L. Dao-Xin, W. Zhan, G. Yang, *Applied surface science*, 257 (2011)  
190 6364-6371.

191 [33] Y. Sasikumar, M. Solomon, L. Olasunkanmi, E. Ebenso, *Materials and Corrosion*,  
192 68 (2017) 776-790.

193 [34] S. Esmailzadeh, M. Aliofkhaezai, H. Sarlak, *Protection of metals and physical*  
194 *chemistry of surfaces*, 54 (2018) 976-989.

195 [35] J.I. Ahuir-Torres, J. Hernández-López, M. Arenas, A. Conde, J. De Damborenea,  
196 *Surface and Coatings Technology*, 259 (2014) 408-414.

197 [36] G. Yi, X. Liu, C. Zheng, H. Zhang, C. Xu, Y.-W. Cui, S. Liu, *Frontiers in*  
198 *Materials*, 7 (2021) 640081.

199 [37] Q. Zhang, B. Duan, Z. Zhang, J. Wang, C. Si, *Journal of Materials Research and*  
200 *Technology*, 11 (2021) 1090-1099.

201 [38] S.L. de Assis, S. Wolyneć, I. Costa, *Electrochimica Acta*, 51 (2006) 1815-1819.

202 [39] R.G. Kelly, J.R. Scully, D. Shoesmith, R.G. Buchheit, *Electrochemical techniques*  
203 *in corrosion science and engineering*, CRC Press, 2002.

204 [40] L.-Y. Chen, H.-Y. Zhang, C. Zheng, H.-Y. Yang, P. Qin, C. Zhao, S. Lu, S.-X.  
205 Liang, L. Chai, L.-C. Zhang, *Materials & Design*, 208 (2021) 109907.

206 [41] F. Endres, S.Z. El Abedin, A. Saad, E. Moustafa, N. Borissenko, W.E. Price, G.G.  
207 Wallace, D.R. Macfarlane, P.J. Newman, A. Bund, *Physical Chemistry Chemical*  
208 *Physics*, 10 (2008) 2189-2199.

209 [42] A. Schmon, K. Aziz, G. Pottlacher, in: *EPJ Web of Conferences*, EDP Sciences,  
210 2017, pp. 04003.

211 [43] V. Bower, R. Davis, T. Murphy, P. Paulsen, J. Gramlich, L. Powell, *JOURNAL*  
212 *OF RESEARCH of the National Bureau of Standards*, 87 (1982) 21.

213 [44] F. Mansfeld, *Corrosion*, 29 (1973) 397-402.

214 [45] A. Toloei, V. Stoilov, D. Northwood, in: *ASME International mechanical*  
215 *engineering congress and exposition*, American Society of Mechanical Engineers, 2013,  
216 pp. V02BT02A054.

217 [46] G. Kear, F.C. Walsh, *Corrosion and materials*, 30 (2005) 51-55.

218 [47] X. Zhang, Z.H. Jiang, Z.P. Yao, Y. Song, Z.D. Wu, *Corrosion Science*, 51 (2009)  
219 581-587.

220 [48] K. Kakaei, M.D. Esrafil, A. Ehsani, *Graphene and anticorrosive properties*, in:  
221 *Interface science and technology*, Elsevier, 2019, pp. 303-337.

222 [49] E. McCafferty, *Introduction to corrosion science*, Springer Science & Business  
223 Media, 2010.

224 [50] K. Leksycki, A. Kaczmarek-Pawelska, K. Ochał, A. Gradzik, D.Y. Pimenov, K.  
225 Giasin, D. Chuchala, S. Wojciechowski, *Materials*, 14 (2021) 6917.

226 [51] I.-J. Hwang, H.-C. Choe, W.A. Brantley, *Surface and Coatings Technology*, 320  
227 (2017) 458-466.

228 [52] M.V. Diamanti, F. Bolzoni, M. Ormellese, E. Pérez-Rosales, M. Pedefferri,  
229 *Corrosion engineering, science and technology*, 45 (2010) 428-434.

230 [53] A. Lasia, *Electrochemical impedance spectroscopy and its applications*, Springer,  
231 2002.

232 [54] J.C. Grotberg, in, *University of Illinois at Chicago*, 2014.

233 [55] M. Holsten, P. Koshy, A. Klink, A. Schwedt, *CIRP Annals*, 67 (2018) 221-224.

234

235